JITH 2017
18èmes Journées Internationales de Thermique (JITH 2017)
Monastir (Tunisie), 25 - 27 Octobre 2017

Influence of Hydrophilic / Hydrophobic Media on the Thermal Metrology: Contribution to Simultaneous Heat and Moisture Transfer

Mohammad AGHAHADI[a, b *], Essolé PADAYODI[b], Saïd ABBOUDI[a],
Laurent ROYON[c], Seyed Amir BAHRANI[d]

[a]ICB, UMR 6303 CNRS, UTBM, Université de Bourgogne Franche-Comté, Belfort , France
[b]ERCOS-ELLIAD, UTBM, Université de Bourgogne Franche-Comté, Belfort
[c]LIED, UMR 8236 CNRS, Université Paris Diderot, Paris
[d]MSC, UMR 7057 CNRS, Université Paris Diderot, Paris

mohammad.aghahadi@utbm.fr
essole.padayodi@utbm.fr
said.abboudi@utbm.fr
laurent.royon@univ-paris-diderot.fr
seyed-amir.bahrani@univ-paris-diderot.fr

Abstract

The present study focuses on thermal metrology of hydrophilic and hydrophobic materials by an experimental approach based on the asymmetric hot plate method and a theoretical approach of coupled heat and humidity transfers. The experimental approach shows that the thermal conductivity of bio-based hydrophilic material increases with humidity (+ 20% when relative humidity RH increases from 30% to 90%, i.e. from 0.028 $\pm 10^{-3}$ to 0.033 $\pm 10^{-3}$ $W.m^{-1}.K^{-1}$ at 20 °C). On the other hand, in the case of a hydrophobic material, such as a phase-change polymer, at the same condition, the measured thermal conductivity is almost constant (0.218 ± 10^{-3} $W.M^{-1}.K^{-1}$). The COMSOL Multiphysics® software is used for computing coupled heat and moisture transfer equations. A good agreement is observed between the numerical and the experimental approaches for the two types of studied materials.

Keywords: Thermal metrology, hot plate method, coupled transfer, hydrophilic, hydrophobic

1. INTRODUCTION

To meet environmental compliance requirements, manufacturers of materials are developing increasingly high-efficient insulators for thermal insulation needs of buildings. Among these, bio-sourced materials offer a double interest in terms of thermal insulating efficiency and low carbon footprint. However, bio-sourced insulators have a major disadvantage related to their behavior in relation to moisture due to their hydrophilicity.

There are different methods for measuring the thermal conductivity of a material. These include the guarded hot plate [1], flash [2], "Hot disc" [3], hot wire [4], hot ribbon [5], tri-layer [6], hot plate methods [7, 8], etc. Among these, the tri-layer and hot plate methods are more suitable for characterizing low thermal conductivity materials such as bio-sourced materials [9,7] or super insulating materials [9].

In the case of hydrophilic materials, such as bio-sourced materials, the measurement of thermal conductivity cannot be carried out with precision without a necessary consideration of the simultaneous transfer of heat and humidity [10].

The objective of this study is to develop a centered hot plate device taking into account the humidity influence so to allow a measurement of the thermophysical properties of a hydrophilic material in a humid environment. This device is validated by numerical results obtained from coupled heat-humidity transfer.

2. EXPERIMENTAL APPROACH

2.1. Hydrophilic and hydrophobic media

Bio-sourced insulating materials are hydrophilic and present a significant porosity. They absorb ambient air moisture over 10% of their dry mass. Thus, in this type of material, the coupling between heat and moisture transfer becomes a necessity.

The hydrophilic/hydrophobic distinction is particularly justified if one is interested in the coupled heat-humidity transfer. Thus, the experimental measurement is carried out on one hand on a hydrophilic material made of flax fibers (LFB) and having high porosity, and on the other hand, on a hydrophobic material, a phase change polymer (PCM) (*Rubitherm® paraffin*) with solidification temperature about 27 °C.

The hydrophilicity or hydrophobicity of these materials is first characterized by the contact angle θ of a water droplet (constant volume) deposited on the sample using a fluid dosing unit and analyzed by means of a CCD camera (*imagine sources*). Second, the hydrophilicity of the wettable material *(when θ<90°)* is then confirmed by the moisture absorption test. This one consists of recording the moisture absorbed by the material when it lies in a hygrometric atmosphere. For this purpose, a sample is previously dried in an oven at 60 °C during 24 h and its dry mass m_0 is accurately weighed. It is then arranged in a climatic chamber (*Dycometal®, CCK 480, Spain*), the atmosphere of which is previously set to a given temperature and humidity and the wet mass $m_h(t)$ of the sample is recorded every 10 min, 30 min or 1 h until the mass does not vary. The humidity absorption rate HAR of the sample is then calculated as [11, 12]:

$$HAR = \frac{(m_h(t) - m_0)}{m_0}.100\ (in\ \%) \qquad (1)$$

Figures 1 and 2 give the results of the contact angle and the water absorption tests, respectively.

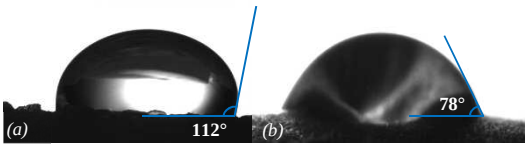

Figure 1: Contact angle (water droplet) on (a) the PCM and (b) the LFB samples

The contact angles θ_{PCM} = 112° ±2° and θ_{LFB} = 78° ±2°, respectively measured on PCM and LFB substrates are averages of five measured values (Fig. 1). The results show that the PCM has a non-wettable surface (as θ_{PCM} > 90°), as the result, this material is hydrophobic. However, LFB has a wettable surface (as θ_{LFB} < 90°) [13] and could be hydrophilic. To confirm this, moisture absorption test is carried out on LFB samples. The first test is performed on 5 samples in an atmosphere at 20°C and 60% of relative humidity (RH) and the second on 4 samples at 40°C and 90% RH. Figure 2 plots curves of the humidity take up.

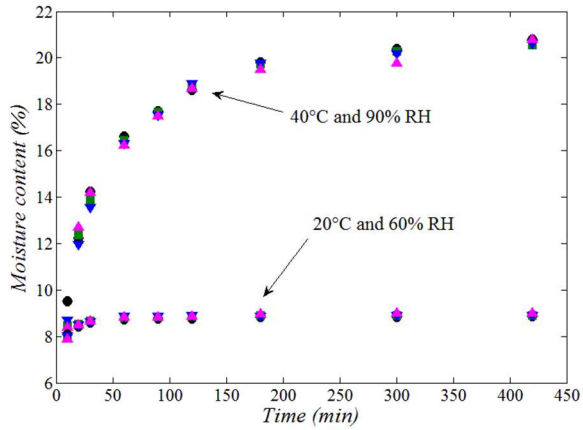

Figure 2: Evolution of humidity absorption of the LFB material

The results show that in theses atmospheres, the LFB material can take up until 9 % *wt* and 21 % *wt* of humidity, respectively. LFB material presents so a high hydrophilicity. Thus, coupling heat and humidity transfer are required for thermal metrology on LFB material.

2.2. Experimental device

The experimental device used for the measurement of the thermal conductivity of the studied samples is the "asymmetrical centered hot plate" [14, 15] (Fig. 3). It consists of a flat heating element of 46 × 46 mm² and 0.15 µm thickness (*Omega®, KHLV-202/10-p, United Kingdom*) and an electrical heating element of about 21 Ω. The heating element is inserted between the sample to characterize and a reference sample with a well-known thermal conductivity ($\lambda_2 = 0.069$ W.m^{-1}.K^{-1}).

The whole system is also inserted between two identical aluminum blocks. K-type thermocouples record the evolution of interfaces temperatures $T_c(t)$, $T_o(t)$ and $T_1(t)$ (Fig. 2). To reduce the contact resistance between substrates, the whole system is compressed with a constant controlled pressure (≈ 6 × 10-2 MPa). The heating element is connected to a power generator (*AIM-TTI®, PLH250-P, UK*) and thermocouples are connected to an acquisition unit (*Omega®, TC-08, UK*).

Measurements are carried out on low-thickness samples (≈ 4 mm) so to allow a unidirectional heat flux across the sample, from one side to the other, and to minimize the lateral heat losses.

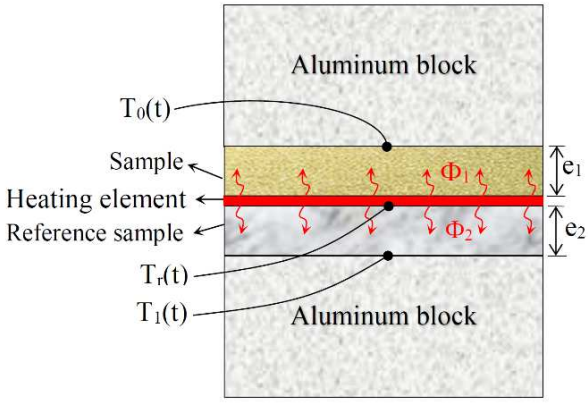

Figure 3: Schematic plan of the asymmetrical centered hot plate.

2.3. Measuring protocol

A heat flow ($\phi = U^2/R.S$) is generated by the heating element by applying to it, a voltage (U=2.33 ± 0.01 V) and a current (I=0.11 ± 0.01 A). The interface temperatures $T_c(t)$, $T_o(t)$ and $T_1(t)$ are then recorded all along the test duration which is sufficiently long to allow thermal exchanges to reach stationary regime (≈3h). By neglecting the lateral heat losses as already explained, the total flux emitted by the heating element (ϕ) is the sum of both heat fluxes ϕ_1 and ϕ_2 , passing through each sample:

$$\phi = \phi_1 + \phi_2 \qquad (2)$$

In a stationary regime, the Fourier's law of heat conduction allows us to write:

$$\begin{cases} \phi_1 = \dfrac{\lambda_1}{e_1}(T_c - T_0) \\ \phi_2 = \dfrac{\lambda_2}{e_2}(T_c - T_1) \end{cases} \qquad (3)$$

The thermal conductivity λ_1 of the sample is deduced from equations (3) as follow:

$$\lambda_1 = \frac{e_1}{T_c - T_0}\left[\frac{U^2}{RS} - \frac{\lambda_2}{e_2}(T_c - T_1)\right] \qquad (4)$$

Since we study thermal exchanges in hydrophilic media in hygrometric environments, the LFB and PCM samples stayed previously about 3 hours in the climatic chamber with controlled humidity and temperature to achieve the hygrothermal equilibrium. The hot plate device provided with samples is then disposed of in the climate Chamber by setting the atmosphere at a given temperature and humidity for all the duration of the measurement.

On the LFB sample, measurements are undertaken at relative humidity conditions of 30%, 50%, 70% and 90% RH, the temperature being maintained for each RH case at 20, 30, 40 and 50 ° C. For the PCM sample, measurements are performed at extreme RH of 30% and 90% and at temperatures below its phase change temperature (27 °C) at 10 and 15 °C.

2.4. Measurement of thermal capacity and absolute density

The thermal capacity and the density are experimentally determined on the LFB and PCM samples. The thermal capacity is measured by the continuous temperature programming method using the DSC calorimeter (*TA Instrument®, Q20, USA*). The measurements are carried out on samples of about 4.3 mg over a temperature range of 5 to 50 °C and with a heating rate of 0.5 °C.min-1. The method is based on the measurement of three thermal fluxes under identical experimental conditions, carried out respectively on the sample to be characterized (ϕ_e), on the reference sample (ϕ_r for distilled water) and at last on empty sample holders (ϕ_b). The thermal capacity of the sample c_{p_e} is then calculated from the correlation:

$$c_{p_e}(T) = c_{p_r}(T)\ \frac{\phi_e - \phi_b}{\phi_r - \phi_b}\ \frac{m_r}{m_e} \qquad (5)$$

Figure 4, shows the thermal capacity evolution of LFB and PCM samples measured experimentally. The thermal capacity of LFB decreases slightly (between 2245 ± 20 J.Kg^{-1}.K^{-1} at 5 °C to 1365 ± 20 J.Kg^{-1}.K^{-1} at 50 °C) while the thermal capacity of PCM is growing significantly in the vicinity of phase change temperature (27 °C).

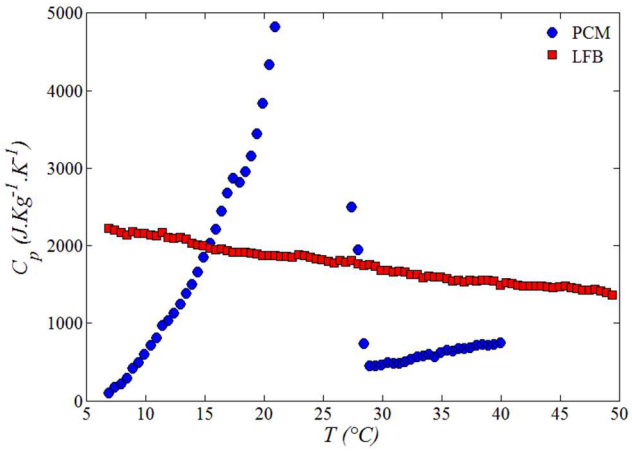

Figure 4: Variation of the heat capacity of PCM and LFB materials according to temperature

The density of samples is determined by a simple method based on the hydrostatic weighing in the ethanol by means of a balance in the ten-thousandth of the gram (*Ohaus®, PA-64, Switzerland*).

3. Modeling of coupled heat and moisture transfer

Within a porous medium in a humid atmosphere, there are three phases: the solid that constitutes the material, the water vapor, and the dry air. Since the solid phase is undeformable and immobile, only the liquid and gaseous phases are considered in the mass balances. Moreover, due to the small dimensions of the pores, it can be considered that the dry air in the gas phase is immobile. When this medium is subjected to a heat source, heat and moisture transfer phenomena occur simultaneously. Different mathematical models that describe the water migration in porous media are proposed in the literature. This phenomenon is induced by the moisture concentration and the temperature gradient during the vapor condensation [16] and a drying process [17]. On a

macroscopic scale, the porous medium can be considered as a homogeneous and continuous medium [17]. The existing water in the pores evaporates on the hot sides, then it moves through the mechanism of diffusion of the gases (we neglect the effect of capillarity in the pores) and condenses on the cold sides. Therefore, we must take into account the latent heat of evaporation in the thermal balance.

The present study proposes a coupled heat and moisture transfer model for the permanent hot plate method where the porous sample is within a humid atmosphere. Mainly the drying process carries out the moisture transfer in the sample. By assuming that the heat capacity C_p of aluminum blocks is so high, so the temperature can be considered constant according to the blocks' thickness. The heat transfer can be assumed to be unidirectional at the center of the sample, according to *Ox* direction (confirmed by results of Fig. 7), as the sample presents a small thickness compared to its lateral dimensions, and regarding the high thermal capacity of the aluminum blocks.

In one-dimensional Cartesian coordinates, the moisture and heat balance equations are:

- *Mass balance (liquid and vapor phases):*

$$\rho_0 \frac{\partial X_l}{\partial t} = \frac{\partial}{\partial x}\left[\rho_0 \left(D_X^l \frac{\partial X_l}{\partial x} + D_T^l \frac{\partial T}{\partial x}\right)\right] - \dot{m} \tag{6}$$

$$\rho_0 \frac{\partial X_v}{\partial t} = \frac{\partial}{\partial x}\left[\rho_0 \left(D_X^v \frac{\partial X_v}{\partial x} + D_T^v \frac{\partial T}{\partial x}\right)\right] + \dot{m} \tag{7}$$

with:

D_X^l : isothermal mass diffusivity on liquid phase ($m^2 s^{-1}$).

D_T^l : non-isothermal mass diffusivity on liquid phase ($m^2 s^{-1} K^{-1}$).

D_X^v : isothermal mass diffusivity on vapor phase ($m^2 s^{-1}$).

D_T^v : non-isothermal mass diffusivity on vapor phase ($m^2 s^{-1} K^{-1}$).

By summing equations (6) and (7), the total mass balance of the two phases is:

$$\frac{\partial X}{\partial t} = \frac{\partial}{\partial x}\left[\left(D_X \frac{\partial X}{\partial x} + D_T \frac{\partial T}{\partial x}\right)\right] \tag{8}$$

where:

$$\begin{aligned} D_X &= D_X^l + D_X^v \\ D_T &= D_T^l + D_T^v \end{aligned} \tag{9}$$

In the vapor phase, by neglecting the accumulation term over the transport term, the quantity of evaporated water per unit of volume of porous medium and per unit of time ($\dot{m}$) is:

$$\dot{m} = -\frac{\partial}{\partial x}\left[\rho_0 \left(D_X^v \frac{\partial X_v}{\partial x} + D_T^v \frac{\partial T}{\partial x}\right)\right] \tag{10}$$

Moreover, by neglecting the thermal diffusion term (D_T^v) over the mass diffusion term (D_X^v) in equation (10), we obtain:

$$\dot{m} = -\frac{\partial}{\partial x} \rho_0 D_X^v \frac{\partial X_v}{\partial x} \tag{11}$$

Figure 5 illustrates the water sorption isotherms [18]. It shows the existence of 3 zones: on the first and second, the water is immobile in the pores. So, we can neglect the mass diffusivity in the liquid phase and consider only the diffusivity in the vapor phase.

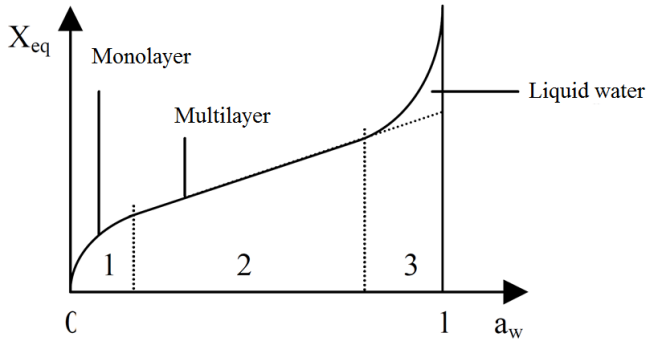

Figure 5: water sorption isotherms

Therefore, by neglecting accumulation term on vapor phase and the thermal diffusion over the mass diffusion, the global mass balance equation is:

$$\frac{\partial X_l}{\partial t} = \frac{\partial}{\partial x}\left[D_X^v \frac{\partial X_v}{\partial x}\right] = \frac{\dot{m}}{\rho_0} \tag{12}$$

- *Heat balance*

On a macroscopic scale, by neglecting the kinetic energy and the assumption that water adsorbed in the pores is not a separate phase and by introducing the heat capacity at constant pressure, the equation of energy is:

$$\rho C_P^* \frac{\partial T}{\partial t} = \frac{\partial}{\partial x}\left[\lambda^* \frac{\partial T}{\partial x} + \rho_0 D_X^v L_v \frac{\partial X_v}{\partial x}\right] \tag{13}$$

Where:

C_P^* is the apparent heat capacity of the porous medium, calculated by:

$$C_P^* = C_{Ps} + X_l C_{Pl} + X_v C_{Pv} + X_a C_{Pa}. \tag{14}$$

L_v is the latent heat of vaporization calculated by:

$$L_v = 2495 - 2.346\,T \tag{15}$$

λ^* is the apparent thermal conductivity, which is given by:

$$\lambda^* = \lambda + \lambda_{dif} \tag{16}$$

The associated initial and boundary conditions are:

- at $t = 0$:

$$\begin{cases} X = X_i \\ \mathrm{T} = T_i \end{cases} \tag{17}$$

The initial mass fraction X_i represents the humidity of a sample when it reaches the hygroscopic equilibrium with the climatic chamber atmosphere. X_i is measured by means of the Desiccator (*Ohaus®, MB-45, Switzerland*).

- at $t > 0\ and\ x = 0$:

$$\begin{cases} \dfrac{\partial X_l}{\partial x} = 0 \\ -\lambda \dfrac{\partial T}{\partial x} = \phi \end{cases} \tag{18}$$

- at $t > 0, x = e_1$

From the aluminum block, the mass transfer flux is null at the interface $x = e_1$ with the sample and assumed isothermal over time, Therefore:

$$\begin{cases} \dfrac{\partial X_l}{\partial x} = 0 \\ T = T_i \end{cases} \qquad (19)$$

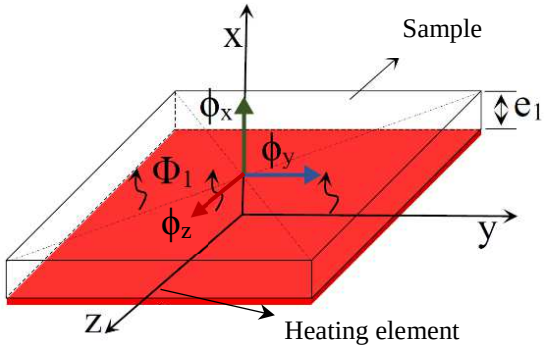

Figure 6: Simplified scheme of hygrothermal transfer media

4. Preliminary results and discussion

4.1. Unidirectional heat flow

To validate the assumption of a unidirectional heat transfer in the center of the sample, the system of equations (8) and (13) with the associated initial and boundary conditions is solved, in tri-dimensional configuration, by COMSOL Multiphysics® software using the experimental parameters listed in Tables 1. The apparent density is measured by dividing the weight of the humid sample by its volume ($\rho^* = {}^{m_h}/_{V_e}$). The isothermal mass diffusivity on vapor phase is a mean of different values of bio sourced materials issue from literature. The obtained result of heat fluxes ϕ_x, ϕ_y *and* ϕ_z according to *Ox*, *Oy and Oz* directions are compared, at the center of the sample, on figure 6. As we see the heat fluxes ϕ_y and ϕ_z are very small compared to the heat flux ϕ_x, which increases up to 27 W.m^{-2} when the hygro-thermal equilibrium is established. This validates the unidirectional heat transfer hypothesis.

Table 1: Measured and estimated values of thermophysical properties

	T (°C) / HR (%)	$\rho_0\ (Kg.m^{-3})$	$C_p{}^*\ (J.Kg^{-1}.K^{-1})$	$\lambda\ (W.m^{-1}.K^{-1})$	X_i	$D_X^v\ (m^2s^{-1})$
PCM	T_i=10(°C) / 90%HR	867	1038	0.201	-	-
	T_i=15(°C) / 90%HR	867	2676	0.217	-	-
LFB	T_i=30(°C) / 30%HR	988	1660	0.030	0.08	2.78×10^{-9}
	T_i=40(°C) / 90%HR	988	1524	0.039	0.17	4.65×10^{-10}

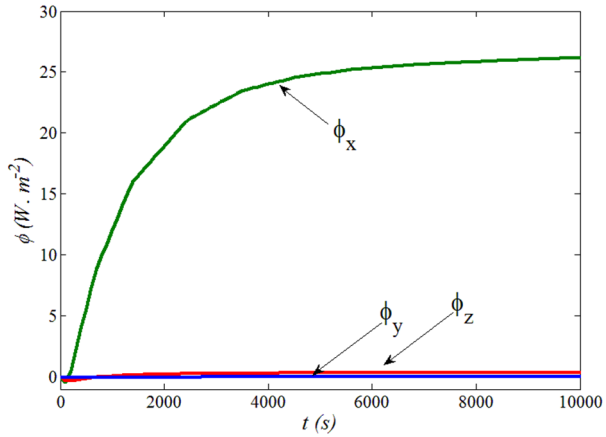

Figure 7: Heat flux variation computed by COMSOL Multiphysics.

4.2. Thermophysical characteristics

At different temperatures and for different relative humidity, experimental measurements of the thermal conductivity are presented in figure 8 for the LFB and on table 2 for the PCM materials, these results are compared to the measurements performed with a commercial apparatus (*TA Instrument®, DTC 300, USA*). The obtained results show a low difference (<2%) with those measured with the hot plate device. Thus, the hot plate device is validated. For the PCM material, the thermal conductivity is measured in two extremes conditions. the climatic chamber is not able to decrease humidity lower than 90% at 10°C, so for low humidity, the inlet water has been cut so that the climatic chamber reaches a balance with the relative humidity of the surrounding area. these results are the average of three measurements in almost identical conditions.

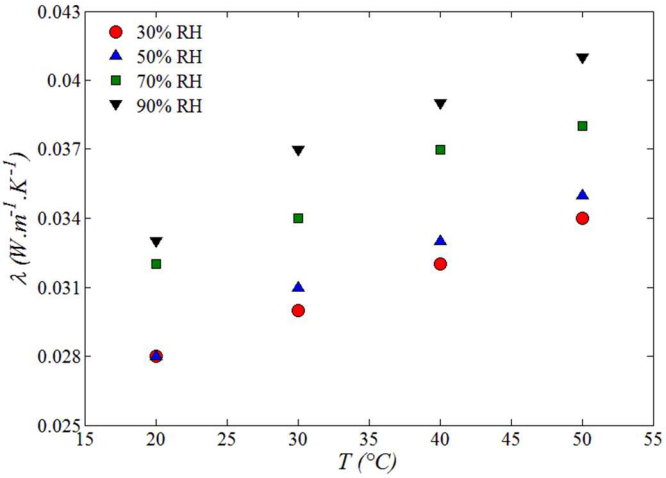

Figure 8: Variation of thermal conductivity of the LFB material as a function of temperature for different relative humidity.

Table 2: Thermal conductivity of the PCM material at different temperatures T_i and relative humidity HR %.

T_i (°C)	RH%	
	30%	90%
	λ ($W.m^{-1}.K^{-1}$) (Uncertainty: $\pm 10^{-3}$)	
10	0.198	0.201
15	0.219	0.217

Figure 8 shows that the thermal conductivity of the hydrophilic material LFB increases as temperature increases (+ 22% when the temperature increases from 20 °C to 50 °C, i.e.). Also as moisture increases (from 30% to 90% RH), the thermal conductivity is increased (from 0.028 $\pm 10^{-3}$ $W.m^{-1}.K^{-1}$ to 0.033$\pm 10^{-3}$ $W.m^{-1}.K^{-1}$) at 20 °C.

Regarding the PCM material, the thermal conductivity increases with the temperature, as might be expected. In an atmosphere at 30% RH, it increases for example from 0.198 $\pm 10^{-3}$ $W.m^{-1}.K^{-1}$ at 10 °C to 0.219$\pm 10^{-3}$ $W.m^{-1}.K^{-1}$ at 15 °C (+ 10% increase). On the other hand, it hardly increases between two extreme values of humidity (30% RH and 90% RH) corroborating thus the inaction of moisture on hydrophobic materials. These results confirm the necessity to take into account the coupled heat and moisture transfer when measuring thermophysical characteristics of hydrophilic materials.

4.3. Numerical results

Figures 9*(a)* and 9*(b)* show a comparison between the experimental and calculated temperatures $\Delta T(t) = T_0(t) - T_i$ on the rear face of the PCM and LFB samples, respectively. In the case of hydrophobic material, the latent heat of vaporization L_v is considered zero, thus the coupling term in the coupled system of equation (13) is canceled. The equation becomes a simple heat transfer problem.

In both cases, a good correlation was observed between the experimental and the numerically simulated curves (variance not exceeding 2%). One can so consider that the proposed coupled heat-moisture transfer model is validated.

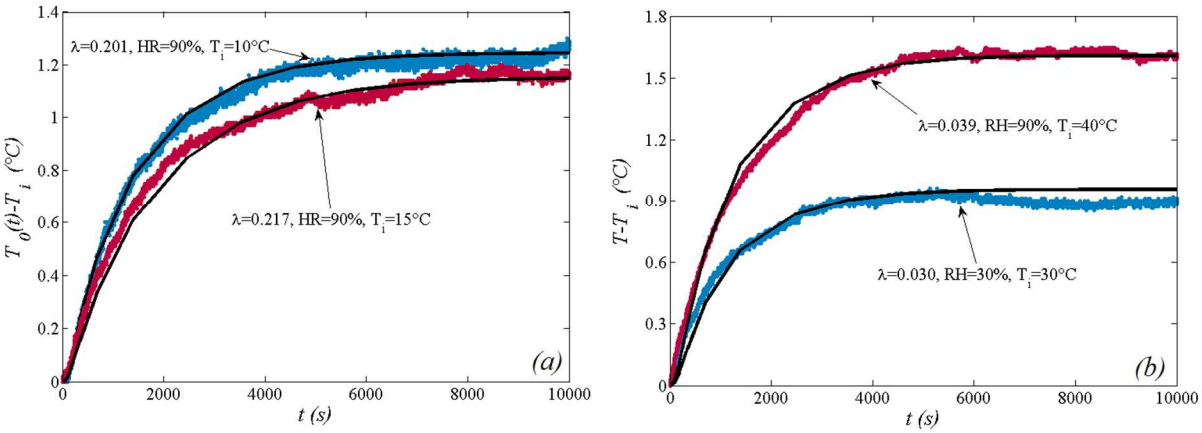

Figure 9: Experimental and calculated temperatures on the rear face of the sample (a) PCM, (b) LFB.

5. Conclusion

In this study, a bio-sourced and a phase change material are considered as a hydrophilic and hydrophobic medium. Humidity adsorption and contact angel investigation confirm the choice of these samples. Then, the coupled heat and moisture transfer are modelized in *1D* Cartesian coordinate by neglecting the mass transfer through the liquid phase. COMSOL Multiphysics® helps us to validate the unidirectional heat transfer hypothesis. In addition, this mathematical model has been solved with this software. The results show a good agreement between the numerical and experimental approaches with a deviation of less than 2%.

The asymmetric hot plate method is then used to measure the thermal conductivity of these materials in a humid atmosphere. At least three measurements are realized in stationary regime. The results show that moisture affects the thermal conductivity of the bio-sourced material while it has no effect on the thermal conductivity of the PCM material.

Nomenclature

Symbols :

C_p Thermal capacity, $J.Kg^{-1}.K^{-1}$
D_X^l Isothermal mass diffusivity on liquid phase, m^2s^{-1}
D_T^l Non-isothermal mass diffusivity on liquid phase, $m^2s^{-1}K^{-1}$
D_X^v Isothermal mass diffusivity on vapor phase, m^2s^{-1}
D_T^v Non-isothermal mass diffusivity on vapor phase, $m^2s^{-1}K^{-1}$
e Thickness, m
HAR Humidity adsorption rate, $\%$
I Current, A
L_v Evaporation latent heat, $KJ.Kg^{-1}$
$\dot{m}$ Quantity of evaporated water per unit volume of the porous medium and per unit of time, $Kg.m^{-3}.s^{-1}$
m Mass, Kg
R Thermal resistance, Ω
S Surface, m^2
T Temperature, $°C$
t Time, s
U Voltage, V
V Volume m^{-3}
X Water vapor mass fraction

Special characters:

θ Contact angle
λ Thermal conductivity, $W.m^{-1}.K^{-1}$
ρ_0 Dry medium density, $Kg.m^{-3}$
ϕ Heat flux, W
Φ Internal heat source, $W.m^{-3}$

Subscripts:

0 Dry
a Air
b Blanc
c Heating element
e Sample
h Humid
i Initial
l Liquid
r Reference
v Water vapor
* Apparent

References

[1] Kobari, T., Okajima, J., Komiya, A., and Maruyama, S., *"Development of guarded hot plate apparatus utilizing Peltier module for precise thermal conductivity measurement of insulation materials,"* Int. J. Heat Mass Transf., vol. 91, pp. 1157–1166, 2015.

[2] Degiovanni, A., Laurent, M., *"Une nouvelle technique d'identification de la diffusivité thermique pour la méthode « flash »,"* Rev. Phys. Appliquée, vol. 21, no. 3, pp. 229–237, 1986.

[3] Jannot, Y., and Acem, Z., *"A quadrupolar complete model of the hot disc,"* Meas. Sci. Technol., vol. 18, no. 5, pp. 1229–1234, 2007.

[4] Andersson, P., *"Thermal conductivity of some rubbers under pressure by the transient hot-wire method,"* J. Appl. Phys., vol. 47, no. 6, pp. 2424–2426, 1976.

[5] Jannot, Y., and Meukam, P., *"Simplified estimation method for the determination of the thermal effusivity and thermal conductivity using a low-cost hot strip,"* Meas. Sci. Technol., vol. 15, pp. 1932–1938, 2004.

[6] Bahrani, S.A., Jannot, Y., and Degiovanni, A., *"Extension and optimization of a three-layer method for the estimation of thermal conductivity of super-insulating materials,"* J. Appl. Phys., vol. 116, no. 14, 2014.

[7] Jannot, Y., Felix, V., and Degiovanni, A., *"A centered hot plate method for measurement of thermal properties of thin insulating materials,"* Meas. Sci. Technol., vol. 21, no. 3, p. 035106, 2010.

[8] Ladevie, B. *"Mise Au Point De Dispositifs De Caracterisation Thermophysique De Materiaux Isolants Solides Ou Pateux."* Ph.D. thesis, 1998.

[9] Félix, V.,*"Caractérisation Thermique de Matériaux Isolants Légers Application à des Aérogels de Faible Poids Moléculaire."* Ph.D. thesis, 2011.

[10] Bal, H., Jannot, Y., Quenette, N., Chenu, A., and Gaye, S., *"Water content dependence of the porosity, density and thermal capacity of laterite based bricks with millet waste additive,"* Constr. Build. Mater. vol. 31, pp. 144–150, 2012.

[11] Atcholi, K-E., Padayodi, E., Sagot, J-C., Beda, T., Samah, O., and Vantomme, J., *"Thermomechanical behavior of the structures of tropical clays from Togo (West Africa) fired at 500 °C, 850 °C and 1060 °C,"* Constr. Build. Mater, vol. 27, pp. 141–148, 2012.

[12] Li, L., Zhou, X., Li, Y., Gong, C., Lu, L., Fu, X., and Tao, W., *"Water absorption and water/fertilizer retention performance of vermiculite modified sulphoaluminate cementitious materials,"* Constr. Build. Mater., vol. 137, pp. 224–233, 2017.

[13] Quere, D., *"Les surfaces super-hydrophobes,"* Images la Phys., pp. 239–244.
[14] Laaroussi, N., Cherki, A., Garoum, M., Khabbazi, A., and Feiz, A., *"Thermal properties of a sample prepared using mixtures of clay bricks,"* Energy Procedia, vol. 42, pp. 337–346, 2013.
[15] Jannot, Y., Degiovanni, A., Grigorova-Moutiers, V., and Godefroy, J., *"A passive guard for low thermal conductivity measurement of small samples by the hot plate method,"* Meas. Sci. Technol., vol. 28, no. 1, p. 15008, 2017.
[16] Bahrani, S.A., Monteau, J. Y., Rezzoug, S. A., Loisel, C., and Maache-Rezzoug, Z., *"Physics-based modeling of simultaneous heat and mass transfer intensification during vacuum steaming processes of starchy material,"* Chem. Eng. Process. Process Intensif., vol. 85, pp. 216–226, 2014.
[17] Moyne, C., and Perre, P., *"Processes related to drying: part I, theoretical model,"* Dry. Technol., vol. 9, no. 5, pp. 1135–1152, 1991.
[18] Jannot, Y., *"Cours d'isotherme de sorption"*, p. 3, 2008